AIP Advances

Elastic behavior of metal-assisted etched Si/SiGe superlattice nanowires containing dislocations

Cite as: AIP Advances **12**, 045006 (2022); https://doi.org/10.1063/5.0084924
Submitted: 11 January 2022 • Accepted: 14 March 2022 • Published Online: 01 April 2022

Nadine Buczek (née Geyer), Michael Hanke, Pawel Buczek, et al.

Elastic behavior of metal-assisted etched Si/SiGe superlattice nanowires containing dislocations

Cite as: AIP Advances 12, 045006 (2022); doi: 10.1063/5.0084924
Submitted: 11 January 2022 • Accepted: 14 March 2022 •
Published Online: 1 April 2022

Nadine Buczek (née Geyer),[1] Michael Hanke,[2,a)] Pawel Buczek,[3] Martin Dubslaff,[2,b)] Alexander A. Tonkikh,[4] Bodo Fuhrmann,[5] and Hartmut S. Leipner[5]

AFFILIATIONS

[1] University of Applied Sciences Lübeck, Mönkhofer Weg 239, 23562 Lübeck, Germany
[2] Paul-Drude-Institut für Festkörperelektronik, Leibniz-Institut im Forschungsverbund Berlin e.V., Hausvogteiplatz 5–7, 10117 Berlin, Germany
[3] Faculty of Engineering and Computer Science, Hamburg University of Applied Sciences, Berliner Tor 7, 20099 Hamburg, Germany
[4] Max-Planck-Institut für Mikrostrukturphysik, Weinberg 2, 06120 Halle (Saale), Germany
[5] Interdisciplinary Center of Materials Science, Martin-Luther-Universität Halle-Wittenberg, Heinrich-Damerow-Straße 4, 01620 Halle, Germany

[a)] **Author to whom correspondence should be addressed:** hanke@pdi-berlin.de
[b)] **Present address:** Bundesamt für Strahlenschutz, Köpenicker Allee 120-130, 10318 Berlin, Germany.

ABSTRACT

We systematically investigate structural parameters, such as shape, size, elastic strain, and relaxations, of metal-assisted etched vertically modulated Si/SiGe superlattice nanowires by using electron microscopy, synchrotron-based x-ray diffraction, and numerical linear elasticity theory. A vertical Si/Ge superlattice with atomically flat interfaces is grown by using molecular beam epitaxy on Si-buffered Si(001) substrates. The lattice constants for Si and Ge are 5.43 and 5.66 Å, respectively, which indicate a lattice mismatch of 4.2%. This results in a strained layer in the boundary between Si and Ge leading to dislocations. These substrates serve as the starting material for nanostructuring the surface by using metal-assisted etching. It is shown that the high quality crystalline structure is preserved in the fabrication process, while the lattice mismatch is partially relieved by dislocation formation. Despite this highly effective relaxation path, dislocations present in the parent superlattice do not vanish upon nanostructuring for wires with diameters of down to at least 80 nm. We relate these observations to the applicability of silicon-based nanowires for high-performance thermoelectric generators.

I. INTRODUCTION

Thermoelectric devices generate electric power directly from heat gradients.[1,2] Avoiding moving parts, they are quiet, long-living, and essentially maintenance-free. Originally deployed on space exploration missions, their potential for harvesting relatively weak renewable energy sources in households and intensively expanding data processing centers is being recognized. The performance of thermometric generators is fundamentally given by the properties of the active material used, described by its figure of merit $ZT = \frac{S^2\sigma T}{\kappa}$ with S, σ, T, and κ, respectively, being the Seebeck coefficient, electrical conductivity, temperature, and thermal conductivity of the material. As such, improvement of the energy conversion efficiency lies in suitable material engineering. First, the intrinsic thermoelectric properties of the parent bulk systems can be improved. Therefore, several strategies have been proposed (see e.g., Ref. 3), including band engineering, the use of spin degrees of freedom, and phonon properties engineering to mention a few. Unfortunately, high performance bulk thermoelectric materials are often toxic and take advantage of scarce elements.

Modification of structural properties has, thus, been put forward as an alternative path for improving the thermoelectric properties. In the bulk phases, introduction of defects can substantially improve the ZT by enhancing phonon

scattering,[4] thus reducing thermal conductivity, and to a lesser extent the power factor σS^2. A similar effect can be achieved through nanostructuring.[5–7] Along these lines, in recent years, nanowires (NWs) fabricated from easily obtainable and non-toxic silicon based parent materials[8] have attracted substantial attention.[9–11]

The information about structural and elastic properties of the wires, especially imperfections, becomes indispensable for the realistic theoretical modeling and the assessment of their thermoelectric performance. In this paper, we report on our structural studies on NWs with built-in Si/Ge superlattices. The lattice constant mismatch in the heterostructure results in the formation of dislocations. One could expect that upon nanostructuring, these dislocations may vanish once the NWs are given the possibility to relax. Here, we show that this scenario is not the case, which, in light of the discussion above, proves to be highly advantageous for thermoelectric applications.

The NWs were obtained by using metal-assisted chemical etching (MACE).[12–15] It is a top-down approach with several important advantages in the context of industrial applications. It allows controllable and cheap fabrication of high quality NWs with easily adjustable diameters down to at least 7 nm. Large areas can be easily and precisely structured. The wires are characterized by a highly crystalline structure, can be easily doped, and are not contaminated with the catalyst because the MACE is typically performed at room temperature.

This paper is organized as follows: first, we provide details concerning the fabrication process of the NWs. They are followed by results of the structural characterization using transmission electron microscopy and x-ray diffraction measurements. Subsequently, numerical simulations of stress and strain distributions based on the finite element method will be presented. The paper ends with an analysis and summary of our findings.

II. NANOWIRE GROWTH

The Si(001) wafer with a Si/SiGe multilayer on top used for the metal-assisted etching was initially grown by the molecular beam epitaxy (MBE) growth as follows: a Si wafer with resistivity in the range of 6–10 Ωcm was RCA-cleaned and then introduced into the MBE reactor (Riber SIVA 45). On top of a Si buffer layer of 200 nm thickness, an undoped Si layer of a thickness of 1.35 nm and, on top of that, an undoped Ge layer with a thickness of 0.57 nm were grown at the growth rates of 0.5 Å/s for Si and 0.2 Å/s for Ge. The growth temperature was maintained at 500 °C. These two layers are repeated 30 times. On top of the multilayer sandwich, a 20 nm thick undoped Si layer was grown. A scheme of this structure is shown in Fig. 1(a).

After the growth of the multilayer, the surface was prepatterned for the metal-assisted chemical etching as follows: in the process of nanosphere lithography, a single layer of monodisperse polystyrene spheres (Microparticles GmbH, Germany) having an average diameter of 390 nm was placed on the wafer surface. Subsequently, the diameter of the polystyrene spheres was reduced by applying oxygen plasma etching, and a 30 nm thick silver film was thermally deposited on the top. Next, the mask of the polystyrene spheres was chemically removed, resulting in a silver hole-mask to appear on top of the heterostructure, cf., Fig. 1(b). Subsequently, the metal-assisted etching of patterned samples was performed. The

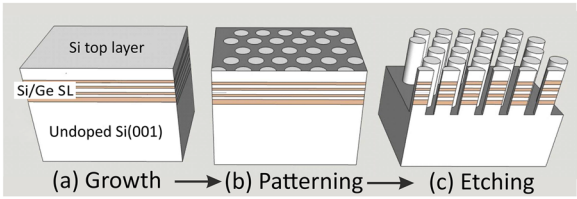

FIG. 1. The schematics of the NW fabrication process: (a) the parent heterostructure used for the NW fabrication hosts a Si/Ge superlattice (SL) with 30 alternating bilayers of 1.35 nm Si and 0.57 nm Ge. It is supported by a 200 nm undoped Si substrate and capped with 20 nm of undoped Si. Following the process of nanosphere lithography, a silver hole-mask has been evaporated onto the surface of the cap (b). Eventually, the NWs emerge in the holes of the mask upon the subsequent etching step (c).

etching solution consisted of 10 ml HF (40 wt. %), 2.5 ml H_2O_2 (30 wt. %), and 37.5 ml H_2O. All samples were etched in the dark at room temperature, resulting in an array of NWs as shown in Fig. 1(c). The details of the preparation and the etching procedures can be found in Ref. 13.

III. RESULTS AND DISCUSSION

The NWs containing a Si/Ge superlattice were subsequently characterized using scanning electron microscopy (SEM) by a XL30 ESEM-FEG (Philips) and transmission electron microscopy (TEM) by a JEM 4010 (JEOL Ltd.), the latter in the plane-section geometry. The results are summarized in Fig. 2. For the two separate samples, the micrographs show ensembles of NWs with diameters of 80 and 200 nm. As a result of the monolithic growth approach, they exhibit a pronounced monodisperse distribution of diameters and lengths within the ensembles. The heterostructure location within the top section of the wires is clearly visible in SEM as it is etched with a higher rate owing to the presence of Ge.[16]

The dislocations appear with a distinct contrast in the weak-beam dark field images as depicted in Figs. 2(c) and 2(f). For the SiGe heterostructures, they possess a misfit characteristic and originate from the lattice mismatch between Si and Ge. The dislocations are clearly observable in the parent material and in the 200 nm as well as 80 nm thick wires (c) and (f). We may remark that the darker lines appearing in (b) and (e) are thickness fringes and bending contours rather than dislocation signatures. Furthermore, in (c), the dislocations are not visible outside the wires as they form primarily at the interface to the substrate. This region is etched off (removed) in the process of nanostructuring.

All x-ray diffraction measurements were performed by using the P08 beamline at the DESY (Hamburg) applying x-ray energy of 8.5 keV with an energy resolution of about 10^{-4}. To probe lateral and vertical mechanical strains in both the systems (the monolithic case vs nanostructured NWs), we have probed complementarily a symmetric (004) and an asymmetric (224) reflection. The first one remains exclusively sensitive to out-of-plane information due to the vanishing in-plane component of the scattering vector q, whereas a non-zero component along the [110] direction provides the in-plane information at the (224) reciprocal lattice point.

Diffusely scattered intensity distributions are plotted in Figs. 3(a)–3(d). In the case of the initial monolithic superlattice, as

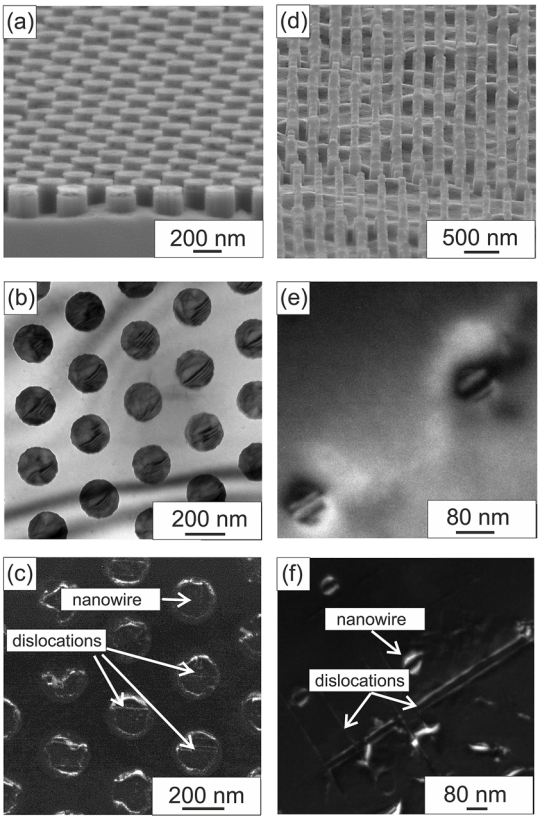

FIG. 2. Electron microscopy images of the investigated NWs. The left and right columns correspond to the wires with diameters of 200 and 80 nm. (a) and (d) depict scanning electron micrographs, while the further are transmission electron micrographs taken as bright field images under two-beam diffraction condition (b) and (e) and as weak-beam dark field images (c) and (f). The bright field images (b) and (e) evidence the presence of penetrating dislocations within both NW ensembles, while the weak-beam dark field image in (f) also contains a signature of dislocations within the parent material.

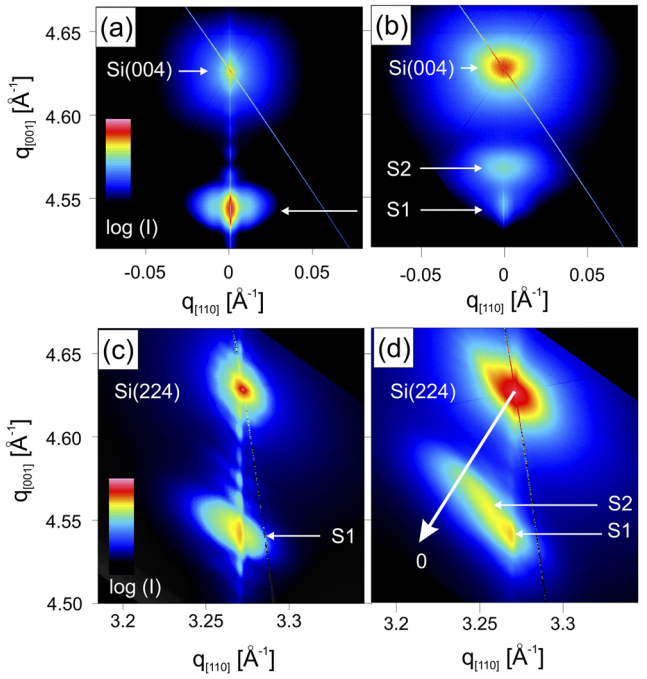

FIG. 3. Synchrotron-based diffusely scattered intensity close to the symmetric and asymmetric Si(004) (a) and (b) and Si (224) (c) and (d) reflections. Both patterns have been taken for the monolithic (a) and (c) and etched structures (b) and (d). The arrow in (d) indicates the direction to the reciprocal origin. Intensity on this line corresponds to fully relaxed unit cells.

shown on the left side, they are close to textbook patterns in which the layer contributions (labeled S1) appear at the same $q_{[110]}$ as the substrate peaks Si(004) and Si(224). This is indicative of a fully pseudomorphic growth, thus identical in-plane lattice constants. Since the Ge lattice constant exceeds the one of Si, the *averaged* value within the superlattice in the vertical growth direction becomes larger compared to pure Si by the experimentally observed value of 1.9%. Assuming a hypothetical SiGe alloy, composed of the same average stoichiometry as the discrete Si/Ge superlattice, one had to approach a composition of $Si_{0.42}Ge_{0.58}$. A lattice mismatch of 4.2% between the pure constituents of the SiGe binary (i.e., Ge and Si) yields then, for the alloy situation, a resulting strain value of about 1.8%, which is very close to the observed one. However, the investigated superlattice consists of discrete slabs of Si and Ge, and consequently, both layers, Si and Ge, are going to be partially strained rather than having a situation where one component, e.g., the Si layers, stays in a bulk-like state while exclusively their counterparts get affected by strain.

Scattering at the etched objects [see Figs. 3(b) and 3(d)] alters the image by another emerging feature (S2) at larger $q_{[001]}$ (at around 4.56 $Å^{-1}$), due to vertically contracted (compared to the unprocessed parent heterostructure) unit cells within the etched NWs. Since the asymmetric reflection Fig. 3(d) becomes sensitive to the in-plane strain, one can see that sample areas related to S2 become laterally relaxed (expanded). However, one notes that the relaxation is not complete, as S2 is not located on the line in the reciprocal space joining the Si(224) reflection with the origin, marked with (0) in Fig. 3(d). The Si/Ge system tends to minimize its elastic energy by keeping the Ge regions contracted at the cost of an expanded Si lattice. This behavior is clearly in line with recent studies of GaInP–InP NWs by using x-ray diffraction (XRD).[17]

Complementary to diffuse x-ray scattering, we have performed numerical Finite Element (FE) calculations based on the linear elasticity theory.[18] Figure 4 depicts the initial FE model (a), the resulting normal components of the elastic strain tensor ε_{xx} and ε_{zz} (c) and (d), and the total strain energy E_{strain}^{total} (b). As expected, the majority of energy is stored primarily within the heteroepitaxial stack, whereas the corresponding elastic strain extends to neighboring areas as well. At the outer boundaries of the NWs, the system can practically fully relax (small deformation), whereas the regions closer to the center are less influenced by the NW surface and are, therefore, subject to higher strain values. Here, the system approaches the limiting case of an infinite two-dimensional layer system. Interestingly, the geometry of the system (aspect ratio of the layer thickness to the NW

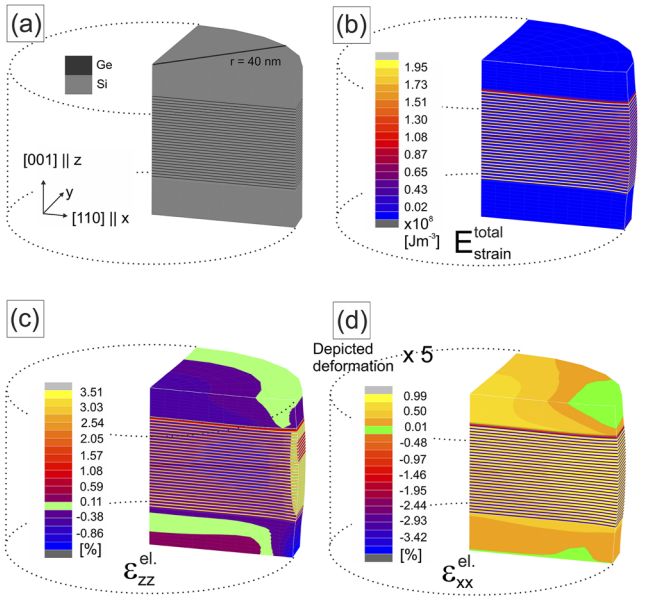

FIG. 4. Finite element calculations of the strain energy distribution (b) and both components of the elastic strain tensor ε_{xx} and ε_{zz} based on the model given in (a). It comprises a Si(001) substrate followed by a vertical sequence of 30 pure Ge/Si bilayers covered by a 20 nm thick capping layer. Due to symmetry, only a quarter of the actual structure has been calculated upon applying the suitable boundary conditions. (c) and (d) depict the calculated deformation within the wires.

diameter) is intermediate between a perfectly layered structure and a very thin NW limit with a fully relaxed lattice.

IV. CONCLUSION

In this study, we have presented a detailed analysis of the elastic behavior of NWs obtained by metal-assisted chemical etching of a parental SiGe heteroepitaxial sequence. The large lateral and vertical strains present in the heterostructure result in misfit dislocations building up in the parent system. Following the process of nanostructuring, the strains partially relax, which, however, do not lead to the disappearance of the dislocations. We observe them for the SiGe NWs with diameters of 200 nm down to 80 nm. These observations are corroborated by the joint x-ray diffraction experiments and linear elastic theory. The geometry of both 200 and 80 nm thick NWs figures in between an infinitely extended two-dimensional layered structure and the ultimate limit of a pure one-dimensional NW with a fully relaxed lattice. Thus, despite the nanostructuring, the NWs offer a limited possibility for the relaxation of the dislocations. In light of the structural investigations presented in this paper, the thermoelectric generators can greatly benefit from the deployment of very thin NWs obtained from layered heterostructures. Both the scattering of the dislocations and the surface phonon scattering can lead to a significant reduction in the thermal conductivity of these systems. At the same time, their high quality crystalline structure is retained, which offers the possibility of preserving the large electrical conductivity of the parent system and, thus, a strong enhancement of the thermoelectric figure of merit.

ACKNOWLEDGMENTS

We thank Peter Werner and Andreas Frommfeld (Max-Planck-Institut für Mikrostrukturphysik, Halle/Saale) for technical support. Beamtime access at the P08 High Resolution Diffraction Beamline at PETRA III (Germany) is highly appreciated.

AUTHOR DECLARATIONS

Conflict of Interest

The authors have no conflicts to disclose.

DATA AVAILABILITY

The data that support the findings of this study are available within the article.

REFERENCES

[1] *CRC Handbook of Thermoelectrics*, edited by D. M. Rowe (CRC, Boca Raton, FL, 1995).
[2] G. J. Snyder and E. S. Toberer, Nat. Mater. **7**, 105–114 (2008).
[3] J. He and T. M. Tritt, Science **357**, eaak9997 (2017).
[4] S. Hu, H. Zhang, S. Xiong, H. Zhang, H. Wang, Y. Chen, S. Volz, and Y. Ni, Phys. Rev. B **100**, 075432 (2019).
[5] C. Gayner, H. Kim, J. Kim, and W. Kim, Mater. Today Energy **12**, 327–335 (2019).
[6] S. Sakane, T. Ishibe, T. Taniguchi, N. Naruse, Y. Mera, T. Fujita, M. M. Alam, K. Sawano, N. Mori, and Y. Nakamura, Mater. Today Energy **13**, 56–63 (2019).
[7] M. Settipalli and S. Neogi, J. Electron. Mater. **49**, 4431–4442 (2020).
[8] Y. Li, G. Wang, M. Akbari-Saatlu, M. Procek, and H. H. Radamson, Front. Mater. **8**, 1 (2021).
[9] R. Chen, J. Lee, W. Lee, and D. Li, Chem. Rev. **119**, 9260–9302 (2019).
[10] I. Donmez Noyan, G. Gadea, M. Salleras, M. Pacios, C. Calaza, A. Stranz, M. Dolcet, A. Morata, A. Tarancon, and L. Fonseca, Nano Energy **57**, 492–499 (2019).
[11] X. Qu and J. Gu, RSC Adv. **10**, 1243–1248 (2020).
[12] N. Geyer, Z. Huang, B. Fuhrmann, S. Grimm, M. Reiche, T.-K. Nguyen-Duc, J. de Boor, H. S. Leipner, P. Werner, and U. Gösele, Nano Lett. **9**, 3106 (2009).
[13] Z. Huang, N. Geyer, P. Werner, J. de Boor, and U. Gösele, Adv. Mater. **23**, 285–308 (2010).
[14] N. Geyer, B. Fuhrmann, H. S. Leipner, and P. Werner, ACS Appl. Mater. Interfaces **5**, 4302 (2013).
[15] A. A. Leonardi, M. J. L. Faro, and A. Irrera, Nanomaterials **11**, 383 (2021).
[16] N. Geyer, N. Wollschläger, B. Fuhrmann, A. Tonkikh, A. Berger, P. Werner, M. Jungmann, R. Krause-Rehberg, and H. S. Leipner, Nanotechnology **26**, 245301 (2015).
[17] S. Hammarberg, V. Dagytė, L. Chayanun, M. O. Hill, A. Wyke, A. Björling, U. Johansson, S. Kalbfleisch, M. Heurlin, L. J. Lauhon, M. T. Borgström, and J. Wallentin, Nano Res. **13**, 2460–2468 (2020).
[18] T. Krause, M. Hanke, O. Brandt, and A. Trampert, Appl. Phys. Lett. **108**, 032103 (2016).